THE JOURNAL OF PHYSICAL CHEMISTRY Letters

Letter

pubs.acs.org/JPCL

Operational Regimes in Picosecond and Femtosecond Pulse-Excited Ultrahigh Vacuum SERS

Eric A. Pozzi,[†] Natalie L. Gruenke,[†,⊥] Naihao Chiang,[§] Dmitry V. Zhdanov,[†] Nan Jiang,[†,∥] Tamar Seideman,[†,§] George C. Schatz,[†] Mark C. Hersam,[†,‡,§] and Richard P. Van Duyne*[,†,§]

[†]Department of Chemistry, [‡]Department of Materials Science and Engineering, and [§]Applied Physics Program, Northwestern University, Evanston, Illinois 60208, United States

Supporting Information

ABSTRACT: We report a systematic study performed in ultrahigh vacuum designed to identify the laser excitation regimes in which plasmonically enhanced ultrashort pulses may be used to nondestructively probe surface-bound molecules. A nondestructive, continuous-wave spectroscopic probe is used to monitor the effects of four different femtosecond- and picosecond-pulsed beams on the SER signals emanating from molecular analytes residing within plasmonically enhanced fields. We identify the roles of plasmonic amplification and alignment with a molecular electronic transition on the observed changes in the SER signals. Our results indicate that overlap of the laser wavelength with the plasmon resonance is the dominant contributor to signal degradation. In addition, signal loss for a given irradiation condition is observed only for molecules residing in hot spots above a threshold enhancement. Identification of suitable laser energy density ranges demonstrates the importance of considering these parameters when implementing SERS in the presence of pulsed irradiation.

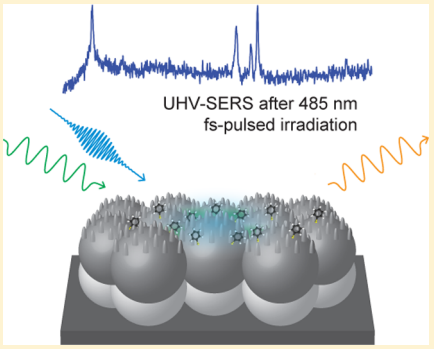

Since the 1980s, scientists have used ultrafast Raman spectroscopic techniques to interrogate the structural dynamics of molecular processes with temporal resolution on the order of femtoseconds—the time scale on which atomic and molecular motion occurs.[1] For example, researchers have used femtosecond stimulated Raman spectroscopy (FSRS) to resolve ultrafast phenomena in systems including green fluorescent proteins,[2] quantum dots,[3] electron donor−acceptor materials,[4−6] and visual pigments.[7] However, in conventional ultrafast spectroscopy, wherein refractive or reflective optics focus light in or on a sample of interest, diffraction of the optical beam prevents spatial resolution below roughly half of the wavelength of light used. Because of this phenomenon, characterized by Ernst Abbe in 1873,[8] features smaller than ∼200 nm cannot be resolved using visible irradiation. A promising means for surpassing this limitation lies in the field of plasmonics.[9] Nanostructured plasmonic materials efficiently confine and amplify far-field irradiation within length scales on the order of several nanometers. In this way, plasmonic nanojunctions, used in the fields of surface-enhanced Raman spectroscopy (SERS) and gap-mode tip-enhanced Raman spectroscopy (TERS), enable the optical diffraction limit to be surpassed.[10]

Recently, researchers have successfully combined ultrafast spectroscopic techniques, such as femtosecond stimulated Raman spectroscopy (FSRS) and coherent anti-Stokes Raman spectroscopy (CARS) with SERS and TERS, enabling ultrafast temporal resolution in addition to high sensitivity.[11−15] However, signal degradation has often been mentioned as a limitation in these studies. A consequence of nanofocusing using plasmonic materials is that the resulting local optical fields are quite intense. Coupled with temporally compressed pulses, which allow molecular dynamics to be temporally resolved, peak electromagnetic (EM) fields can reach levels that damage molecules.[16] Molecules are especially susceptible to decomposition upon electronic excitation, a situation that occurs when the wavelength of light overlaps with a molecular electronic transition. In this resonance condition, intense EM fields can induce rapid decay of the sample in a photobleaching process.[17] Several demonstrations of induced signal loss from plasmonic cavities irradiated with ultrashort pulses have been reported,[12,16,18,19] but investigations evaluating the physical phenomena responsible for decay of signal in plasmonically enhanced ultrafast spectroscopy remain incomplete.

In this Letter, we identify the influences of frequency overlap between ultrashort pulses and system resonances on SER signal stability in ultrahigh vacuum (UHV). We consider the roles of molecular and plasmon resonances and conduct power dependence studies to determine the intensity regimes in which these resonances affect SERS behavior. In addition, we analyze the resulting SER spectra after high-intensity irradiation to address the remaining enhancing capability of the SERS substrate and the fate of molecules whose SERS response is lost.

Received: May 26, 2016
Accepted: July 18, 2016

DOI: 10.1021/acs.jpclett.6b01151
J. Phys. Chem. Lett. 2016, 7, 2971−2976

Probing the effects of ultrafast irradiation on molecular adsorbates and plasmonic substrates can be difficult due to the nanoscale nature of the experiments. SERS, however, is a convenient and useful tool for probing ultrafast beam-induced damage to molecules and plasmonic nanostructures. The character and magnitude of the SER signal provide valuable information about molecular structure, which can change as a result of degradation, and plasmonic enhancement, which may be affected by damage to the plasmonic substrate or separation between molecules and substrate. Therefore, we systematically monitor the effects of ultrafast irradiation using SERS to investigate the regimes in which these phenomena operate.

Before a discussion about the effects of ultrafast irradiation on UHV-SER signals, we must properly address the resonances involved. Specifically, we must identify the overlap of plasmonic and molecular resonances with the four pulsed beams used in this study: narrow-band 795 nm (~1 ps, abbr. ps795), broad-band 800 nm (~50 fs, abbr. fs800), 525 nm (~225 fs, abbr. fs525), and 485 nm (~225 fs, abbr. fs485). Alignment with one or both resonances (molecular or plasmonic) may provide pathways leading to SER signal loss.

Overlap of the excitation wavelength with the substrate localized surface plasmon resonance (LSPR) must be taken into account, since the locally intense electromagnetic fields may damage molecules and/or the substrates themselves. The Ag film-over-nanospheres (AgFON) substrates used here exhibited LSPRs in the range 530−560 nm as identified through surface reflectance measurements (Figure 1A). Photons absorbed or scattered by the substrate result in a dip in the surface reflectance, which is indicative of the LSPR spectral position. For all AgFONs used, the LSPR overlapped most strongly with the fs525 beam, with considerable overlap with the fs485 beam evident in each case. The near-IR beams, ps795 and fs800, coincide with the edge of the reflectance dip and therefore had minimal overlap with the LSPR of each substrate.

For this study, two molecules with differing electronic resonances were chosen: rhodamine 6G (R6G) and benzenethiol (BT) (Figure 1B,C). R6G absorbs strongly in the green, whereas BT has no absorption features in the visible.[20] Specifically, the electronic resonance of surface-bound R6G is centered near 540 nm, and absorption is appreciable between ca. 470 and 570 nm.[21−23] R6G then is strongly resonant with the fs525 beam, partially on-resonant with the fs485 beam, and off-resonant with the ps795 and fs800 beams, while BT is off-resonant with all excitation sources.

To investigate the influences of ultrashort pulse energies and intensities on UHV-SER signals, we carried out systematic power-dependent investigations using each ultrafast beam. An illustration of the experimental schematic is presented in Figure 1D. Briefly, a 532 nm continuous-wave (CW) beam constantly irradiated the sample and probed the SERS response without inducing any photochemical response or signal degradation. This beam was confirmed to be nonperturbing through sequential spectral acquisitions prior to the start of the experiment. Subsequently, a sequence of 10 1 s spectra was first collected to mark the initial SERS intensity. The sample was then irradiated for 10 s with the ultrafast beam, after which 10 additional 1 s spectra were collected using the CW probe. This step was repeated three more times to probe the extent of signal decay after repeated irradiation events.

Signal behavior for both R6G and BT are plotted in Figure 2. In constructing these plots, only the signals before and after the

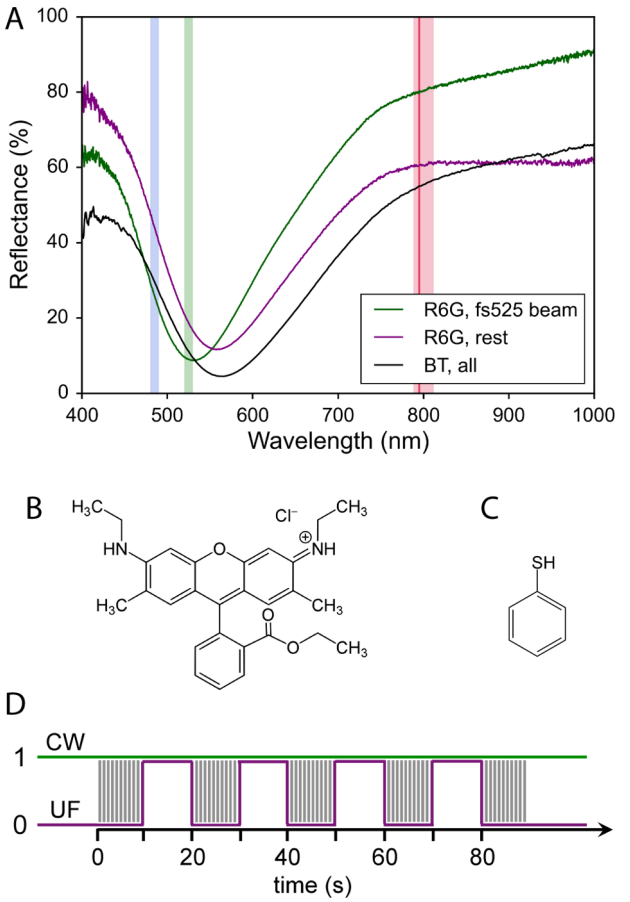

Figure 1. (A) The surface extinction spectra of the AgFONs depict the localized surface plasmon resonance (LSPR) of each substrate used. For R6G experiments, the green spectrum represents the substrate used with the fs525 beam, and the purple spectrum represents the substrate used for the other pulsed beams. The black spectrum represents the substrate used for BT experiments for all pulsed beams. Shaded vertical bands represent the wavelengths and approximate spectral widths of the ultrafast beams used as a guide to illustrate conditions on and off the plasmon resonance. (B,C) Molecular structures of (B) R6G and (C) BT. (D) Time-domain experimental schematic, in which "1" designates on and "0" designates off. Vertical gray lines denote 1 s spectral acquisitions.

first pulsed irradiation were considered, with I/I_0 representing the portion of the SERS intensity remaining. For the sake of comparison, we will quantify a signal decay midpoint, SD50, as the laser power required to reduce the UHV-SER signal by 50%. Signal decays on the semilog plots were empirically fit with sigmoidal curves for objective identification of SD50 at the inflection point of each fit. In the case of R6G (Figure 2A), the near-IR beams did not induce signal decay at any of the powers used, whereas the fs485 and fs525 beams induced signal loss with signal decay midpoints $SD50_{fs485}$ = 3.4 × 10^{-5} J cm^{-2} $pulse^{-1}$ (9.3 × 10^{-5} W) and $SD50_{fs525}$ = 2.8 × 10^{-5} J cm^{-2} $pulse^{-1}$ (7.7 × 10^{-5} W). However, since both of these beams overlap with the electronic resonance of R6G as well as the LSPR (Figure 1A), it is unclear which resonance contributes to the observed signal loss.

To separate the effects of molecular and plasmonic resonances on the observed signal loss, we analyzed BT UHV-SER signal damage under analogous experimental conditions (Figure 2B). Although BT is not resonant with any of the lasers used, signal decay midpoints were observed at

DOI: 10.1021/acs.jpclett.6b01151
J. Phys. Chem. Lett. 2016, 7, 2971−2976

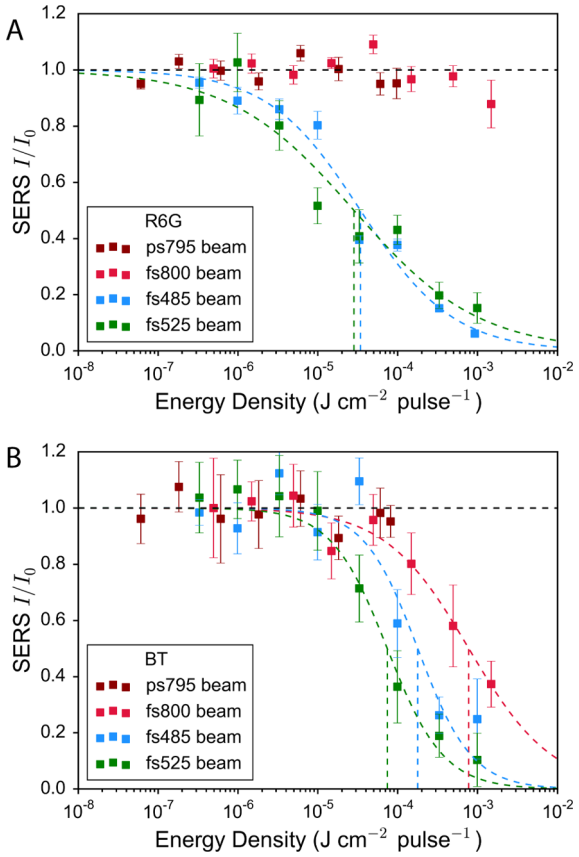

Figure 2. Proportion of SERS intensity remaining after the first 10 s of ultrafast irradiation for (A) R6G and (B) BT. Data are displayed corresponding to each pulsed laser beam, and data are fit to sigmoidal curves to extract the signal decay midpoint, SD50 ($I/I_0 = 0.5$), denoted by vertical dashed lines, for each molecule/laser combination.

comparable irradiation intensities to those observed for R6G, indicating that the plasmon resonance of the substrate is responsible for the majority of the observed signal loss. Confirming this notion, greater overlap of the beam energy with the LSPR (Figure 1A) correlates with a downshifted SD50; the signal decay midpoint for the strongly overlapping fs525 beam lies at 7.4×10^{-5} J cm^{-2} pulse^{-1} (2.0×10^{-4} W), whereas that for the moderately overlapping fs485 beam and the largely off-resonant fs800 beam lie at 1.8×10^{-4} J cm^{-2} pulse^{-1} (4.9×10^{-4} W) and 7.8×10^{-4} J cm^{-2} pulse^{-1} (1.4×10^{-3} W), respectively. We will demonstrate later in this report that signal loss results from a molecular mechanism as opposed to damage to the plasmonic substrate.

We must also consider heat induced by pulsed irradiation in the discussion of signal loss. In the Supporting Information we outline calculations for the expected increase in temperature per pulse, which should not exceed ~15 K for the energy densities used. Further, we consider heat dissipation both along the Ag film and into the silica spheres. Heat dissipation along the Ag film is expected to dominate, and the resulting temperature increase will not exceed approximately 60 K. A temperature increase of this magnitude will not desorb or decompose either R6G or BT on the AgFON substrate.

While the substrate LSPR appears to be the dominant contributor to signal damage, SD50 differs between R6G and BT for a given ultrafast beam. Notably, SD50 is lower for R6G with visible pulsed beams than for BT. We attribute this observation to the fact that R6G physisorbs to Ag and is known to diffuse across the Ag surface.[19,24] Signal loss can therefore arise from thermal diffusion or desorption of R6G away from SERS hot spots, mechanisms that chemisorbed BT is unlikely to undergo. It is also possible that surface-bound R6G photobleaches under resonant excitation.[25] This possibility is minimized in the UHV environment, but there is no direct experimental proof to completely rule out photobleaching. We note that R6G and BT were investigated on separate AgFON substrates, and differing magnitudes of surface enhancement may lead to variances in SD50 values. In addition, alignment with the molecular resonance of R6G may play a secondary role in signal decay.

It is important to note that the UHV-SER signal intensities did not degrade unless irradiated with pulses with durations on the femtosecond time scale as opposed to the picosecond time scale. The peak intensities within ultrashort pulses therefore must be considered when planning experiments. Curiously, the fs800 beam was observed to induce decay for BT but not for R6G. A likely reason for this observation lies in the degree of overlap of the fs800 beam with the AgFON LSPR. While subtle, the differences in the surface-averaged plasmonic properties of each investigated AgFON result in a marked variance in signal behavior under NIR irradiation. As depicted in Figure 1A, the LSPR for the AgFON used for BT UHV-SERS with fs800 irradiation extends further into the near-IR than does the LSPR for the AgFON used for R6G with the same pulsed beam. Differences in signal behavior between R6G and BT under fs800 irradiation can then be understood by considering slight variability among AgFON substrates. Specifically, BT signal loss under fs800 irradiation is consistent with greater plasmonic enhancement at 800 nm on the BT-functionalized AgFON in comparison to the R6G-functionalized AgFON. However, this difference in signal behavior may not be as large as it seems; given that BT exhibits signal decay only under the highest fs800 energy densities used, the equivalent SD50 for R6G could lie only a couple orders of magnitude higher than that for BT and would not be observed given our experimental parameters.

SERS behavior after subsequent pulsed irradiation events was then analyzed to determine the extent of signal decay with continued irradiation. Specifically, we seek to resolve whether or not the signal will continue to decrease by an equivalent fraction after each irradiation. Alternatively, the signal may stabilize with nonzero intensity, corresponding to molecules residing at "cold" sites, wherein the enhanced electromagnetic field is insufficient to cause signal loss regardless of the duration of irradiation. From the plotted I/I_0 ratios after further irradiation events, the latter is clearly the case (Figure 3). This result is in agreement with the report by Dlott and co-workers, who used laser pulses with increasing field intensity to probe the distribution of local field enhancements on the same AgFON SERS substrates used in the current study.[16] The authors found that systematically increasing pulse intensities resulted in photochemical damage of molecules residing at surface sites with progressively lower enhancements. Additionally, prolonged irradiation with a given intensity did not induce signal decay from molecules residing at surface sites with enhancements below a threshold value. This phenomenon is consistent with the broad, long-tail distribution of enhancements present among hot spots in SERS.[26] We note that it is difficult to discount the existence of a second exponential decay mechanism operating at time scales much slower than the

DOI: 10.1021/acs.jpclett.6b01151
J. Phys. Chem. Lett. 2016, 7, 2971−2976

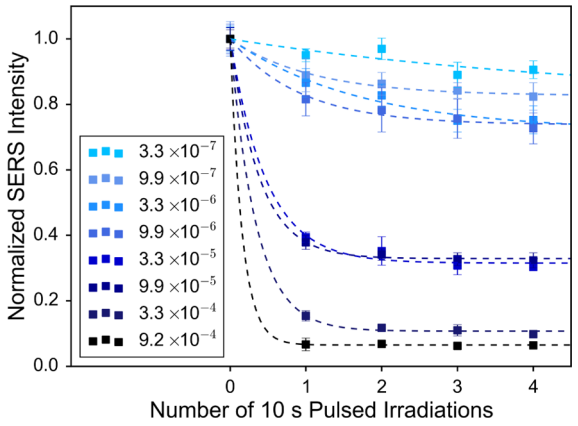

Figure 3. Plots of remaining R6G SERS intensity after subsequent 10-s periods of fs485 pulsed irradiation. The legend refers to laser power densities with units J cm^{-2} pulse^{-1}. For each power density, data are fit to exponential curves decaying to a nonzero constant.

duration of the current experiment. However, given the similarity between our results and those from the Dlott group,[16] we expect that a single-exponential decay mechanism is valid.

Analysis of the spectra after the observation of significant photodamage provides insight into the nature of the damage. Plots of representative spectra of R6G and BT before and after high-intensity irradiation are depicted in Figure 4. Upon loss of R6G signal, no additional features appear. This observation may either evidence (a) substrate damage resulting in a loss of enhancement, (b) molecular damage resulting in fragments that are not visible in the collected spectra due to a loss of resonance enhancement, or (c) diffusion or desorption of R6G away from the irradiated hot spots. More generally, mechanism (a) describes damage to the plasmonic substrate, whereas mechanisms (b) and (c) describe perturbation only to the molecules. In principle, one could evaluate the presence or absence of mechanism (a) through irradiation of the bare AgFON prior to molecular deposition. However, the difficulty in relocating a previously irradiated area of the surface after molecular deposition limits the practicality of this approach.

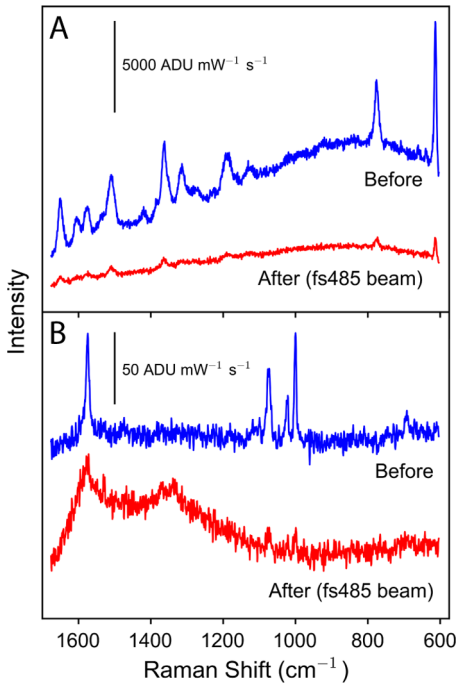

Figure 4. Representative SER spectra before and after damage. (A) SERS of R6G before and after one 10 s irradiation of the fs485 beam with 3.3 × 10^{-4} J cm^{-2} pulse^{-1}. (B) SERS of BT before and after one 10 s irradiation with 9.9 × 10^{-4} J cm^{-2} pulse^{-1}.

Mechanism (c) is a distinct possibility for R6G. However, given that signal loss is evident for BT, which is chemisorbed to the Ag surface and encased in an alumina capping layer, we conclude that there is another mechanism at play because mechanism (c) cannot fully explain the BT results. Since R6G has an atypically high Raman cross section and is additionally resonantly enhanced at the probe wavelength of 532 nm, one would expect signals from R6G fragments to be appreciably weaker than those from R6G; thus, mechanism (b) cannot be ruled out in the case of R6G. In contrast, spectra of BT after irradiation display a loss of BT peaks concurrent with a rise in a carbonaceous background signal[27,28] of non-negligible intensity. No additional beam-induced spectral features are observed. BT and amorphous carbon scattering are found to be strongly anticorrelated (Figure S1, Supporting Information), consistent with a molecular decay mechanism (mechanism (b)). Given that the amorphous carbon signal is observed with appreciable intensity, we conclude that the plasmonic activity of the AgFON SERS substrates remains after pulsed irradiation for the pulse energy densities used in this study. We then anticipate that mechanism (a) stated above is not applicable to the BT studies and, by extension, the R6G measurements in this study; in other words, signal loss is not a result of damage to the SERS substrates in the cases of both R6G and BT. Thus, we conclude that mechanism (b) is responsible for loss of BT signal and that loss of R6G signal results from mechanisms (b) and/or (c).

However, these results are also not completely general. We expect experimental parameters, such as the photostability of the molecule under study, the enhancement factor and plasmonic spectral position of the SERS substrate, and the environment of the experiment to alter the signal loss regimes in a given study. For example, SE-FSRS experiments have shown signal loss beginning at around 10^{-6} J cm^{-2} pulse^{-1} for the same ps795 beam used in these experiments combined with a beam similar to the fs800 beam used here.[12] Instead, we observed no damage due to the ps795 or fs800 beams at that energy density. We attribute this observation to the lack of a vacuum environment in SE-FSRS in addition to the red-shifted plasmon resonance frequency of the Au nanoantennas used in the SE-FSRS study in comparison with that of the AgFONs used here. Nevertheless, while the signal decay midpoints we establish here may not hold for every ultrafast SERS experiment, they highlight the importance of studying signal loss and carefully designing plasmonically enhanced ultrafast studies to avoid molecular and plasmonic degradation. They also provide insights into potential degradation mechanisms specific to UHV studies.

We have demonstrated that the frequency overlap between the pulsed laser beam and the substrate LSPR is the most critical component to signal decay when combining ultrafast irradiation with plasmonic enhancement. When irradiation energy is aligned with the LSPR of the enhancing substrate, modest power densities can result in molecular damage due to the combined effects of electromagnetic enhancement and high peak power during pulses. This effect becomes more critical as pulse duration decreases. Therefore, it is important to consider

DOI: 10.1021/acs.jpclett.6b01151
J. Phys. Chem. Lett. 2016, 7, 2971−2976

the enhancement factor of SER substrates for each wavelength of ultrafast irradiation used in plasmonically enhanced ultrafast spectroscopy along with laser energy densities. We also conclude that there is a threshold hot spot strength, below which continued irradiation of a given wavelength and energy density will not induce signal decay from adsorbed molecules. By sweeping the intensity of each laser by over 3 orders of magnitude we have identified signal decay midpoints at laser pulse energy densities in the range of 10^{-5} to 10^{-3} J cm^{-2} $pulse^{-1}$. This study demonstrates the necessity to identify damage regimes in plasmonically enhanced spectroscopy in the presence of ultrafast irradiation and provides insight into the rational design of time-resolved studies in the field of plasmonics.

EXPERIMENTAL METHODS

AgFON substrates were fabricated by drop-casting 390 nm silica spheres onto silicon wafers, onto which a 200−250 nm Ag film was evaporated in a manner previously described.[29,30] Substrates were designed to exhibit maximal enhancement with 532 nm irradiation. For studies on R6G, AgFONs were brought into the UHV through a load lock, where they were thermally degassed above 100 C overnight prior to use. R6G was deposited onto the AgFONs through sublimation,[24] after which the substrates were placed in the optical path for experimentation. For studies on BT, a AgFON substrate was incubated in 1 mM BT in ethanol for 6 h before being thoroughly rinsed. An alumina capping layer was deposited using atomic layer deposition (ALD) in a manner reported previously[31] to prevent thiol contamination of the UHV chamber. Twenty cycles of alternating doses of trimethylaluminum (10 min exposure) and H_2O using ultrahigh purity N_2 as the carrier gas (2 min exposure) provided a capping layer roughly 2.2 nm thick.[32] The substrate was then brought into UHV and placed in the optical path without further treatment.

UHV-SERS was performed using the same instrument previously described,[33] with a base pressure of $\sim 2 \times 10^{-11}$ Torr. Optics external to the chamber (focal length, 100 mm) focused and collected light at an angle of ∼75° with respect to the sample normal. Incident light was s-polarized with respect to the sample plane. Collected light was then focused on the entrance slit of the spectrograph (Princeton Instruments SCT 320) and detected using a thermoelectrically cooled charge coupled device (Princeton Instruments Pixis 400). Chamber pressure remained below 1×10^{-10} Torr throughout all measurements.

Pulsed beams were generated by a femtosecond regenerative amplifier (Coherent RegA 9050, 100 kHz, 1W, 800 nm, 50 fs) seeded by a Ti:sapphire oscillator (Coherent Micra, 80 MHz, 400 mW, 800 nm, 30 fs).[12] The amplifier and oscillator are both pumped by an 18 W, 532 nm pump laser (Coherent Verdi V18). Half of the fundamental output of the RegA served as the fs800 beam. To form the ps795 beam, the fs800 beam was passed through a pair of narrow bandpass filters (CVI Laser Optics, F1.5−794.7), resulting in a beam with a pulse duration of approximately 1 ps. An optical parametric amplifier (Coherent OPA 9450, 20 mW, 225 fs) was pumped with the remaining half of the RegA fundamental. The OPA output was tuned to either 485 or 525 nm to create the fs485 and fs525 beams, respectively. All beams were inserted into the common optical path into the UHV chamber using a 90/10 plate beamsplitter (Chroma 21011) and attenuated using neutral density filters to obtain the desired powers as measured in the optical path prior to the chamber entrance. SER signal intensities were quantified using the integrated area of the 612 and 1574 cm^{-1} peaks of R6G and BT, respectively. For each adsorbate, equivalent signal behavior was observed for all measured peaks.

To determine energy densities, all beams were characterized outside of the UHV chamber using a beam profiler (Ophir NS2-Si/3.5/1.8-PRO). After focusing with the 100 mm focal length lens used in this study, the ps795, fs800, fs525, and fs485 beams were measured to have $1/e^2$ diameters ($x \times y$) of 70 × 70 μm, 30 × 20 μm, 30 × 30 μm, and 30 × 30 μm, respectively. The focused 532 nm CW probe (Spectra-Physics Excelsior) had a measured diameter of 10 × 10 μm, ensuring that the entire probe area was contained within the area of each pulsed beam. These measured diameters and the ∼75° angle of incidence with respect to the sample normal were taken into account when evaluating the probe area of each beam to properly calculate power densities.

ASSOCIATED CONTENT

Supporting Information

The Supporting Information is available free of charge on the ACS Publications website at DOI: 10.1021/acs.jpclett.6b01151.

Plot of the statistical correlation of BT UHV-SER spectra and calculations of expected temperature increase per pulse and heat dissipation (PDF)

AUTHOR INFORMATION

Corresponding Author

*E-mail: vanduyne@northwestern.edu.

Present Addresses

[⊥]N.L.G.: Department of Chemistry, University of California, Berkeley, CA 94720, United States and Molecular Biophysics and Integrated Bioimaging Division, Lawrence Berkeley National Laboratory, Berkeley, CA 94720, United States.

[∥]N.J.: Department of Chemistry, University of Illinois Chicago, Chicago, IL 60607, United States.

Notes

The authors declare no competing financial interest.

ACKNOWLEDGMENTS

E.A.P., N.L.G., G.C.S., and R.P.V.D. acknowledge support from the National Science Foundation Center for Chemical Innovation dedicated to Chemistry at the Space−Time Limit (CaSTL) Grant CHE-1414466. N.C., N.J., M.C.H., and R.P.V.D. acknowledge funding from the Department of Energy Office of Basic Energy Sciences (SISGR Grant DE-FG02-09ER16109). T.S. acknowledges funding from the NSF under grant CHE-1465201. E.A.P., G.C.S., M.C.H., and R.P.V.D. acknowledge further support from the National Science Foundation Materials Research Science and Engineering Center (DMR-1121262). E.A.P. and N.L.G. were additionally supported by the National Science Foundation Graduate Research Fellowship under Grant DGE-1324585.

REFERENCES

(1) Zewail, A. H. Femtochemistry: Atomic-Scale Dynamics of the Chemical Bond. *J. Phys. Chem. A* **2000**, *104*, 5660−5694.

(2) Fang, C.; Frontiera, R. R.; Tran, R.; Mathies, R. A. Mapping GFP Structure Evolution During Proton Transfer with Femtosecond Raman Spectroscopy. *Nature* **2009**, *462*, 200−204.

DOI: 10.1021/acs.jpclett.6b01151
J. Phys. Chem. Lett. 2016, 7, 2971−2976

(3) Hannah, D. C.; Brown, K. E.; Young, R. M.; Wasielewski, M. R.; Schatz, G. C.; Co, D. T.; Schaller, R. D. Direct Measurement of Lattice Dynamics and Optical Phonon Excitation in Semiconductor Nanocrystals Using Femtosecond Stimulated Raman Spectroscopy. *Phys. Rev. Lett.* **2013**, *111*, 107401.
(4) Brown, K. E.; Veldkamp, B. S.; Co, D. T.; Wasielewski, M. R. Vibrational Dynamics of a Perylene−Perylenediimide Donor−Acceptor Dyad Probed with Femtosecond Stimulated Raman Spectroscopy. *J. Phys. Chem. Lett.* **2012**, *3*, 2362−2366.
(5) Frontiera, R. R.; Dasgupta, J.; Mathies, R. A. Probing Interfacial Electron Transfer in Coumarin 343 Sensitized TiO2 Nanoparticles with Femtosecond Stimulated Raman. *J. Am. Chem. Soc.* **2009**, *131*, 15630−15632.
(6) Lockard, J. V.; Butler Ricks, A.; Co, D. T.; Wasielewski, M. R. Interrogating the Intramolecular Charge-Transfer State of a Julolidine−Anthracene Donor−Acceptor Molecule with Femtosecond Stimulated Raman Spectroscopy. *J. Phys. Chem. Lett.* **2010**, *1*, 215−218.
(7) Kukura, P.; McCamant, D. W.; Yoon, S.; Wandschneider, D. B.; Mathies, R. A. Structural Observation of the Primary Isomerization in Vision with Femtosecond-Stimulated Raman. *Science* **2005**, *310*, 1006−1009.
(8) Abbe, E. Beiträge Zur Theorie Des Mikroskops Und Der Mikroskopischen Wahrnehmung. *Arch. Mikrosk. Anat.* **1873**, *9*, 413−418.
(9) Stiles, P. L.; Dieringer, J. A.; Shah, N. C.; Van Duyne, R. P. Surface-Enhanced Raman Spectroscopy. *Annu. Rev. Anal. Chem.* **2008**, *1*, 601−626.
(10) Sonntag, M. D.; Klingsporn, J. M.; Zrimsek, A. B.; Sharma, B.; Ruvuna, L. K.; Van Duyne, R. P. Molecular Plasmonics for Nanoscale Spectroscopy. *Chem. Soc. Rev.* **2014**, *43*, 1230−1247.
(11) Gruenke, N. L.; Cardinal, M. F.; McAnally, M. O.; Frontiera, R. R.; Schatz, G. C.; Van Duyne, R. P. Ultrafast and Nonlinear Surface-Enhanced Raman Spectroscopy. *Chem. Soc. Rev.* **2016**, *45*, 2263−2290.
(12) Frontiera, R. R.; Henry, A.-I.; Gruenke, N. L.; Van Duyne, R. P. Surface-Enhanced Femtosecond Stimulated Raman Spectroscopy. *J. Phys. Chem. Lett.* **2011**, *2*, 1199−1203.
(13) Yampolsky, S.; Fishman, D. A.; Dey, S.; Hulkko, E.; Banik, M.; Potma, E. O.; Apkarian, V. A. Seeing a Single Molecule Vibrate through Time-Resolved Coherent Anti-Stokes Raman Scattering. *Nat. Photonics* **2014**, *8*, 650−656.
(14) Zhang, Y.; Zhen, Y.-R.; Neumann, O.; Day, J. K.; Nordlander, P.; Halas, N. J. Coherent Anti-Stokes Raman Scattering with Single-Molecule Sensitivity Using a Plasmonic Fano Resonance. *Nat. Commun.* **2014**, *5*, 4424.
(15) Hua, X.; Voronine, D. V.; Ballmann, C. W.; Sinyukov, A. M.; Sokolov, A. V.; Scully, M. O. Nature of Surface-Enhanced Coherent Raman Scattering. *Phys. Rev. A: At., Mol., Opt. Phys.* **2014**, *89*, 043841.
(16) Fang, Y.; Seong, N.-H.; Dlott, D. D. Measurement of the Distribution of Site Enhancements in Surface-Enhanced Raman Scattering. *Science* **2008**, *321*, 388−392.
(17) Etchegoin, P. G.; Lacharmoise, P. D.; Le Ru, E. C. Influence of Photostability on Single-Molecule Surface Enhanced Raman Scattering Enhancement Factors. *Anal. Chem.* **2009**, *81*, 682−688.
(18) Klingsporn, J. M.; Sonntag, M. D.; Seideman, T.; Van Duyne, R. P. Tip-Enhanced Raman Spectroscopy with Picosecond Pulses. *J. Phys. Chem. Lett.* **2014**, *5*, 106−110.
(19) Pozzi, E. A.; Sonntag, M. D.; Jiang, N.; Chiang, N.; Seideman, T.; Hersam, M. C.; Van Duyne, R. P. Ultrahigh Vacuum Tip-Enhanced Raman Spectroscopy with Picosecond Excitation. *J. Phys. Chem. Lett.* **2014**, *5*, 2657−2661.
(20) Biggs, K. B.; Camden, J. P.; Anker, J. N.; Van Duyne, R. P. Surface-Enhanced Raman Spectroscopy of Benzenethiol Adsorbed from the Gas Phase onto Silver Film over Nanosphere Surfaces: Determination of the Sticking Probability and Detection Limit Time. *J. Phys. Chem. A* **2009**, *113*, 4581−4586.
(21) Zhao, J.; Jensen, L.; Sung, J.; Zou, S.; Schatz, G. C.; Van Duyne, R. P. Interaction of Plasmon and Molecular Resonances for Rhodamine 6G Adsorbed on Silver Nanoparticles. *J. Am. Chem. Soc.* **2007**, *129*, 7647−7656.
(22) Dieringer, J. A.; Wustholz, K. L.; Masiello, D. J.; Camden, J. P.; Kleinman, S. L.; Schatz, G. C.; Van Duyne, R. P. Surface-Enhanced Raman Excitation Spectroscopy of a Single Rhodamine 6G Molecule. *J. Am. Chem. Soc.* **2009**, *131*, 849−854.
(23) Darby, B. L.; Auguié, B.; Meyer, M.; Pantoja, A. E.; Le Ru, E. C. Modified Optical Absorption of Molecules on Metallic Nanoparticles at Sub-Monolayer Coverage. *Nat. Photonics* **2016**, *10*, 40−45.
(24) Klingsporn, J. M.; Jiang, N.; Pozzi, E. A.; Sonntag, M. D.; Chulhai, D.; Seideman, T.; Jensen, L.; Hersam, M. C.; Van Duyne, R. P. Intramolecular Insight into Adsorbate−Substrate Interactions Via Low-Temperature, Ultrahigh-Vacuum Tip-Enhanced Raman Spectroscopy. *J. Am. Chem. Soc.* **2014**, *136*, 3881−3887.
(25) Galloway, C. M.; Artur, C.; Grand, J.; Le Ru, E. C. Photobleaching of Fluorophores on the Surface of Nanoantennas. *J. Phys. Chem. C* **2014**, *118*, 28820−28830.
(26) Le Ru, E. C.; Etchegoin, P. G.; Meyer, M. Enhancement Factor Distribution around a Single Surface-Enhanced Raman Scattering Hot Spot and Its Relation to Single Molecule Detection. *J. Chem. Phys.* **2006**, *125*, 204701.
(27) Yoshikawa, M.; Katagiri, G.; Ishida, H.; Ishitani, A.; Akamatsu, T. Raman Spectra of Diamondlike Amorphous Carbon Films. *J. Appl. Phys.* **1988**, *64*, 6464−6468.
(28) Kudelski, A.; Pettinger, B. SERS on Carbon Chain Segments: Monitoring Locally Surface Chemistry. *Chem. Phys. Lett.* **2000**, *321*, 356−362.
(29) Hulteen, J. C.; Treichel, D. A.; Smith, M. T.; Duval, M. L.; Jensen, T. R.; Van Duyne, R. P. Nanosphere Lithography: Size-Tunable Silver Nanoparticle and Surface Cluster Arrays. *J. Phys. Chem. B* **1999**, *103*, 3854−3863.
(30) Greeneltch, N. G.; Blaber, M. G.; Henry, A.-I.; Schatz, G. C.; Van Duyne, R. P. Immobilized Nanorod Assemblies: Fabrication and Understanding of Large Area Surface-Enhanced Raman Spectroscopy Substrates. *Anal. Chem.* **2013**, *85*, 2297−2303.
(31) Masango, S. S.; Hackler, R. A.; Henry, A.-I.; McAnally, M. O.; Schatz, G. C.; Stair, P. C.; Van Duyne, R. P. Probing the Chemistry of Alumina Atomic Layer Deposition Using Operando Surface-Enhanced Raman Spectroscopy. *J. Phys. Chem. C* **2016**, *120*, 3822−3833.
(32) Ott, A. W.; Klaus, J. W.; Johnson, J. M.; George, S. M. Al3O3 Thin Film Growth on Si(100) Using Binary Reaction Sequence Chemistry. *Thin Solid Films* **1997**, *292*, 135−144.
(33) Jiang, N.; Foley, E. T.; Klingsporn, J. M.; Sonntag, M. D.; Valley, N. A.; Dieringer, J. A.; Seideman, T.; Schatz, G. C.; Hersam, M. C.; Van Duyne, R. P. Observation of Multiple Vibrational Modes in Ultrahigh Vacuum Tip-Enhanced Raman Spectroscopy Combined with Molecular-Resolution Scanning Tunneling Microscopy. *Nano Lett.* **2012**, *12*, 5061−5067.

DOI: 10.1021/acs.jpclett.6b01151
J. Phys. Chem. Lett. 2016, 7, 2971−2976